

Bridging Sensor Gaps via Attention Gated Tuning for Hyperspectral Image Classification^{*}

Xizhe Xue^a, Haokui Zhang^{a,b}, Rong Xiao^b, Ying Li^{a,*}, Zongwen Bai^c and Mike Zheng Shou^d

^aNational Engineering Laboratory for Integrated Aero-Space-Ground-Ocean Big Data Application Technology, Shaanxi Provincial Key Laboratory of Speech & Image Information Processing, Northwestern Polytechnical University., Xi'an, China

^bIntellifusion, Shenzhen, China

^cSchool of Physics and Electronic Information, Yan'an University., Yan'an, China

^dDepartment of Electrical and Computer Engineering, National University of Singapore, Singapore

ARTICLE INFO

Keywords:

hyperspectral image classification
cross-sensor tuning
attention gated tuning
vision transformer
triplet-structured transformer

ABSTRACT

Data-hungry HSI classification methods require high-quality labeled HSIs, which are often costly to obtain. This characteristic limits the performance potential of data-driven methods when dealing with limited annotated samples. Bridging the domain gap between data acquired from different sensors allows us to utilize abundant labeled data across sensors to break this bottleneck. In this paper, we propose a novel Attention-Gated Tuning (AGT) strategy and a triplet-structured transformer model, Tri-Former, to address this issue. The AGT strategy serves as a bridge, allowing us to leverage existing labeled HSI datasets, even RGB datasets to enhance the performance on new HSI datasets with limited samples. Instead of inserting additional parameters inside the basic model, we train a lightweight auxiliary branch that takes intermediate features as input from the basic model and makes predictions. The proposed AGT resolves conflicts between heterogeneous and even cross-modal data by suppressing the disturbing information and enhances the useful information through a soft gate. Additionally, we introduce Tri-Former, a triplet-structured transformer with a spectral-spatial separation design that enhances parameter utilization and computational efficiency, enabling easier and flexible fine-tuning. Comparison experiments conducted on three representative HSI datasets captured by different sensors demonstrate the proposed Tri-Former achieves better performance compared to several state-of-the-art methods. Homologous, heterologous and cross-modal tuning experiments verified the effectiveness of the proposed AGT. Code has been released at: <https://github.com/Cecilia-xue/AGT>.

1. Introduction

Hyperspectral image (HSI) contains rich spectral information about the composition and properties of objects, resulting in a wide range of applications in earth observation, e.g., mineral exploration Carrino et al. (2018), plant stress detection Behmann et al. (2014), and environmental science Tranon et al. (2018), etc. Within these applications, HSI classification technology identifies each pixel in an image and assign it to a specific land-cover category. Over the past decade, deep learning (DL) based methods Lin et al. (2013); Chen et al. (2014, 2015); Zhang et al. (2017); Li et al. (2017); Chen et al. (2016); Zhang et al. (2021) dominate the field of HSI classification. From 2013 until now, various optimized convolutional neural networks (ConvNets) have been proposed for HSI classification Zhang et al. (2017); Li et al. (2017); Chen et al. (2016). Among them, 3D ConvNet-based HSI classification methods have become the mainstream in this field, because the 3D convolution is inherently well-suited for processing the HSI with 3D structure. Recently, the emergence of the vision transformer (ViT) has disrupted this situation and researchers have begun exploring how to apply ViT models to handle the HSI classification task. Hong *et al.* Hong et al. (2021) were the first to apply pure transformers to HSI classification. In the same trend, impressive results have been achieved by combining the transformer with ConvNet Sun et al. (2022), architecture search (NAS) algorithm Xue et al. (2022) and new absolute position embedding Jiang et al. (2024).

^{*} This work was supported in part by the National Natural Science Foundation of China (62271400) and the Key R & D projects of Shaanxi Province, China (2023-GHZD-02).

^{*}Corresponding author

✉ xuexizhe@mail.nwpu.edu.cn (X. Xue); hkzhang@nwpu.edu.cn (H. Zhang); rongxiao@gmail.com (R. Xiao); lybyp@nwpu.edu.cn (Y. Li); ydbzw@yau.edu.cn (Z. Bai); mike.zheng.shou@gmail.com (M.Z. Shou)
ORCID(s): 0000-0001-8636-3993 (X. Xue)

The performance of aforementioned data-hungry methods are closely related to the quantity and quality of labeled data. However, annotating HSIs requires field surveys by professionals, making the process time-consuming and expensive. The number of labeled hyperspectral data is relatively small. To alleviate this problem, some early work Zhang et al. (2019); Yang et al. (2017) explores how to use additional labelled data from other domains to further push back these limits. Two-CNN-transfer Yang et al. (2017) first investigates transfer learning between the data from the same sensor in HSI classification. On similar trend, Zhang et al. (2019) concentrates on exploiting data from other sensors and transferring the knowledge. Such previous work Zhang et al. (2019); Yang et al. (2017) both bridge the domain gap between source and target domains by fine tuning the ConvNets. However, such fine tuning methods do not perform effectively enough when meeting the transformer architecture. Because ConvNets optimize convolutional filter parameters during training, while transformer architectures learn specific pixel relationships within the training data. Compared with ConvNets, the transformer-based models are always more sensitive to the characteristics of the training data. Given these differing learning approaches, the fine tuning transfer learning strategies proposed for ConvNet-based methods are not able to be directly applied to the transformer framework. Although some recent approaches Gao et al. (2021); Hu et al. (2022); Sung et al. (2022) have been proposed to the transformer architectures, they cannot learn domain-invariant features effectively on HSIs. Because HSI datasets acquired by various sensors display distinct structural characteristics. Tuning methods designed for unimodal RGB images cannot takes advantage of the cross-modal discrepancies and handle the gaps between cross-sensor HSIs well.

In this paper, we aim to address this challenge by optimizing the external tuning strategy and internal architecture of the model. Externally, we advocate that a good representation of the target features should not only contain the knowledge from the source domain but also preserve the target-domain-specific information. Therefore, we analyze the relationships between different sensors and propose an attention-gated tuning strategy (AGT) to reconcile conflicts in heterogeneous and cross-modal data. Specifically, we introduce a lightweight parallel auxiliary branch for the target dataset, enabling information exchange with the basic model through an attention-gated tuning block. This block uses guidance signals from the auxiliary branch and semantic information from the basic model to suppress noise and enhance relevant features, facilitating effective model tuning. Internally, for efficient feature learning from limited annotated samples, we focus on enhancing parameter utilization and flexibility in architecture design. We analyze the spatial-spectral characteristics of HSI and introduce Tri-Former, a flexible spectral-spatial separation transformer tailored for HSI classification. Tri-Former also employs 3D convolutions to enhance structural information. Our proposed method demonstrates promising performance across all three representative HSI datasets, showcasing its effectiveness in addressing the challenges of HSI classification.

The main contributions of this paper are outlined as follows.

1. A novel Attention-Gated Tuning (AGT) strategy is proposed for transformer-based HSI classification methods to address conflicts in cross-sensor and even cross-modality data.
2. A triplet-structured HSI classification transformer, Tri-Former, is designed after analyzing the characteristics of HSI. Tri-Former's flexible architecture enables efficient feature transfer learning from relatively limited training samples.
3. This work establishes a connection between RGB and HSI datasets, allowing for the utilization of abundant RGB labeled datasets to enhance HSI classification performance, especially in scenarios with limited labeled HSI data.

The remaining sections of this paper are structured as follows. Section 2 presents a review of related work. In Section 3, we provide a detailed explanation of our proposed Tri-Former model and AGT strategy. Algorithm implementation details are outlined in Section 4, followed by an extensive evaluation and comparison with state-of-the-art competitors. Finally, in Section 5, we conclude this work.

2. Related Work

2.1. ConvNets for Hyperspectral Image Classification

ConvNets Krizhevsky et al. (2012); Simonyan and Zisserman (2014); Szegedy et al. (2017); He et al. (2016); Huang et al. (2017); Howard et al. (2017); Liu et al. (2022) emerged as a powerful tool for visual classification, revolutionizing the field by shifting focus from handcrafted features to data-driven architecture design. The adeptness of convolutional networks in feature extraction perfectly aligns with the demands of hyperspectral image classification. The emergence

of convolutional networks has also revolutionized the field of HSI classification, elevating the accuracy of classification to a new level.

Over the past decade, various convolutional variants have been proposed for HSI classification. 1D ConvNet and 2D ConvNet are first introduced into HSI classification. Mei and Ling Mei et al. (2016); Zhang and Li (2016) employed 1D ConvNets to perform convolution along the spectral dimension, effectively extracting spectral features. Meanwhile, a series of HSI classification approaches Makantasis et al. (2015); Yue et al. (2015) based on 2D ConvNet have been proposed. 1D ConvNet considers spectral dimension, while 2D ConvNet always focuses on spatial dimension. Later, researchers pursued dual-channel ConvNet structures after recognizing the potential of combining spectral and spatial information. Zhang et al. Zhang et al. (2017) and Yang et al. Yang et al. (2017) introduced dual-channel ConvNet models that effectively integrated 1D ConvNet and 2D ConvNet, achieving further improvements in accuracy for HSI classification. Since 2016, 3D ConvNet based methods have become the mainstream as 3D convolution naturally extracts spectral-spatial features from 3D HSIs. Li et al. Li et al. (2017) and Chen et al. Chen et al. (2016) pioneered this approach, constructing 3D ConvNet architectures to capture spatial-spectral patterns efficiently. The inherent 3D nature of HSIs was leveraged, enabling comprehensive feature extraction and improving classification performance. After that, researchers mainly focus on designing HSI characteristic-aligned 3D ConvNets. Efficient residual structures were introduced by Zhong et al. Zhong et al. (2018), integrating spectral and spatial residual modules to improve feature learning. Zhang et al. Zhang et al. (2019) focused on lightweight 3D-CNN designs and transfer learning strategies to handle small sample problems. Getting inspiration from DARTS, Chen et al. Chen et al. (2019) proposed a 3D Auto-CNN for HSI classification. In the preprocessing stage, 3D Auto-CNN heavily compresses the spectral dimension of raw HSIs through point wise convolution. Under this basis, 3DANAS Zhang et al. (2021) and HyT-NAS Xue et al. (2022) are designed, which introduce the NAS algorithm into an efficient 3D pixel-to-pixel classification framework.

The evolution of ConvNet-based HSI classification methods embodies three fundamental principles, including: 1) simultaneously harnessing spectral and spatial information contributes to enhancing accuracy; 2) the 3D convolution operation is inherently well-suited for processing 3D HSI; 3) aligning the classification framework with the inherent characteristics of HSI is unignorable. These three guiding principles have been adhered to in the conception of the Tri-Former model.

2.2. Vision Transformers for Hyperspectral Image Classification

Transformer model was initially introduced for Natural Language Processing (NLP) by Vaswani et al. Vaswani et al. (2017). It brought about a revolutionary change in processing sequential data through its attention mechanism. In the field of computer vision, ViT Dosovitskiy et al. (2020) builds on the success of the transformer, which was originally designed for NLP.

More recently, within the HSI classification domain, researchers have redirected their focus towards the transformer model in their quest for enhanced performance Hong et al. (2021); He et al. (2021); Qing et al. (2021). For instance, He et al. He et al. (2021) introduced a spatial-spectral transformer that combines a ConvNet for capturing spatial information with a ViT for extracting spectral relationships. Similarly, the method proposed in Qing et al. (2021) adopts a spectral relationship extraction transformer along with several decoders. SpectralFormer Hong et al. (2021) mines and represents the sequence attributes of spectral signatures well from input HSIs using the transformer model. It extracts spectrally local sequence information from neighboring bands of HSIs. Meanwhile, HyT-NAS Xue et al. (2022) first combines the NAS and transformer for handling the HSI classification task. An emerging transformer module is grafted on the automatically designed ConvNet to add global information to local region focused features. The searching space in HyT-NAS is hybrid, suitable for the HSI data with a relatively low spatial resolution and an extremely high spectral resolution. To better utilize high-level semantic spectral-spatial features, a spectral-spatial feature tokenization transformer (SSFTT) method Sun et al. (2022) is proposed. Specifically, a spectral-spatial feature extraction module is built to extract low-level shallow features and a gaussian weighted feature tokenizer is introduced for feature transformation. Based on this, the transformed features are input into the transformer encoder module for stronger feature representation and learning. Another model GraphGST Jiang et al. (2024) incorporates a new absolute positional encoding (APE) to capture pixel positional sequences and uses self-supervised learning for cross-view contrastive learning, improving representation and capturing local-to-global correlations in HSI classification tasks.

The methods mentioned above have shown the transformer's potential in effectively leveraging spatial and spectral relationships within hyperspectral data. However, there is still significant room for improvement. In this paper, we further enhance the intrinsic strengths of the transformer architecture in HSI classification by improving its parameter utilization and flexibility.

2.3. Fine Tuning Methods

In real-world scenarios, obtaining a sufficient amount of training data for HSI classification is challenging due to the expensive sensor cost and labeling cost. Therefore, designing models with low training sample requirements has consistently been a goal within the HSI classification domain. A classical approach to addressing this challenge is to pretrain the method on the sufficiently labeled data (maybe from another domain) first, and then transfer the acquired knowledge and representations to the target domain Pan and Yang (2009).

Fine Tuning ConvNets in HSI classification. As a pioneering effort to address HSI classification problems with limited training samples, Yang *et al.* Yang *et al.* (2017) introduced the transfer learning strategy into a two-branch ConvNet to extract more relevant features from HSIs. In Zhang *et al.* (2019), Zhang *et al.* further improved this idea and transferred feature extraction capacity among heterogeneous HSI datasets and even cross-modal datasets. Unfortunately, these methods may not exhibit effective performance on transformer architecture. In LWNet Zhang *et al.* (2019) and Two-CNN Yang *et al.* (2017), fine tuning strategies are employed on ConvNet architectures, yielding promising results. However, unlike ConvNets, which learn convolutional filter parameters from extensive datasets, transformer-based methods learn specific pixel relationships within the training data. Given these differing learning approaches, the fine tuning transfer learning strategy used in ConvNet-based methods exhibit limited effectiveness in the transformer framework.

Full-Parameter Fine Tuning. Due to the rapid advancements in vision language models, an increasing number of fine tuning methods targeting transformer architectures have been proposed. As shown in Figure 1(a), Full Parameter Fine Tuning (FPFT) adjusts all layers and parameters based on the pre-trained model to adapt it to a specific task. This process usually uses a small learning rate and task-specific data to fully utilize the general features of the pre-trained model, but may require more computing resources.

Parameter-Efficient Fine Tuning. Parameter-Efficient Fine Tuning (PEFT) technology aims to improve the performance of pre-trained models on new tasks by minimizing the number of fine tuning parameters and computational complexity. In this way, even if computing resources are limited, the knowledge of the pre-trained model can be used to quickly adapt to new tasks and achieve efficient transfer learning. Therefore, PEFT technology can greatly shorten the model training time and computational cost while improving the model effect, allowing more people to participate in deep learning research. A popular line of work on PEFT is to add a few trainable parameters without changing the original parameters of the pre-trained model. Figure 1(b)-Figure 1(e) illustrate the information forward and gradient backpropagation process of some representative PEFT approaches. Adapter tuning Gao *et al.* (2021) approaches always insert small neural network modules, called "adapters", between each layer of the model or between certain specific layers. These adapters are trainable, while the parameters of the original model remain unchanged. Similar to Adapter tuning, LoRA Hu *et al.* (2022) adds small, low-rank matrices to the key layers of the model to adjust the model's behavior. Prompt tuning Lester *et al.* (2021) adds learnable embedding vectors as prompts to the input of the pre-trained language model. These prompts are designed to be updated during training to guide the model to output more useful responses for specific tasks. Without inserting additional parameters inside backbone networks, another line of work on PEFT is to add an additional small and separate network. Zhang *et al.* Zhang *et al.* (2020) proposed Side-tuning, which adapts a pre-trained network by training a lightweight "side" network that is fused with the (unchanged) pre-trained network via summation. In a similar trend, LST Sung *et al.* (2022) trains a ladder side network. This small and separate network takes intermediate activations as input via shortcut connections (called ladders) from backbone networks and makes predictions.

In this paper, in order to make full use of labeled cross-sensor data, we propose an attention-gated tuning (AGT) strategy and employ it to finetune the proposed efficient Tri-Former. The proposed approach demonstrates effectiveness across homogeneous, heterogeneous, and even cross-modality cases. Although the proposed AGT takes inspiration and has a similar parallel structure to LST, we argue that there are major differences in motivations, key problems and architecture designs between the two methods. Detail comparisons and comprehensive analysis are presented in Section 4.3. The corresponding experimental results are outlined in Section 4.6-4.8.

3. Proposed Method

In this section, we provide a detailed introduction to the proposed Tri-Former model and AGT strategy. We start by giving a concise overview of the vanilla visual transformer architecture before diving into the architecture of our Tri-Former model. Following that, we elaborate on the details of the AGT strategy, emphasizing its differences from previous approaches.

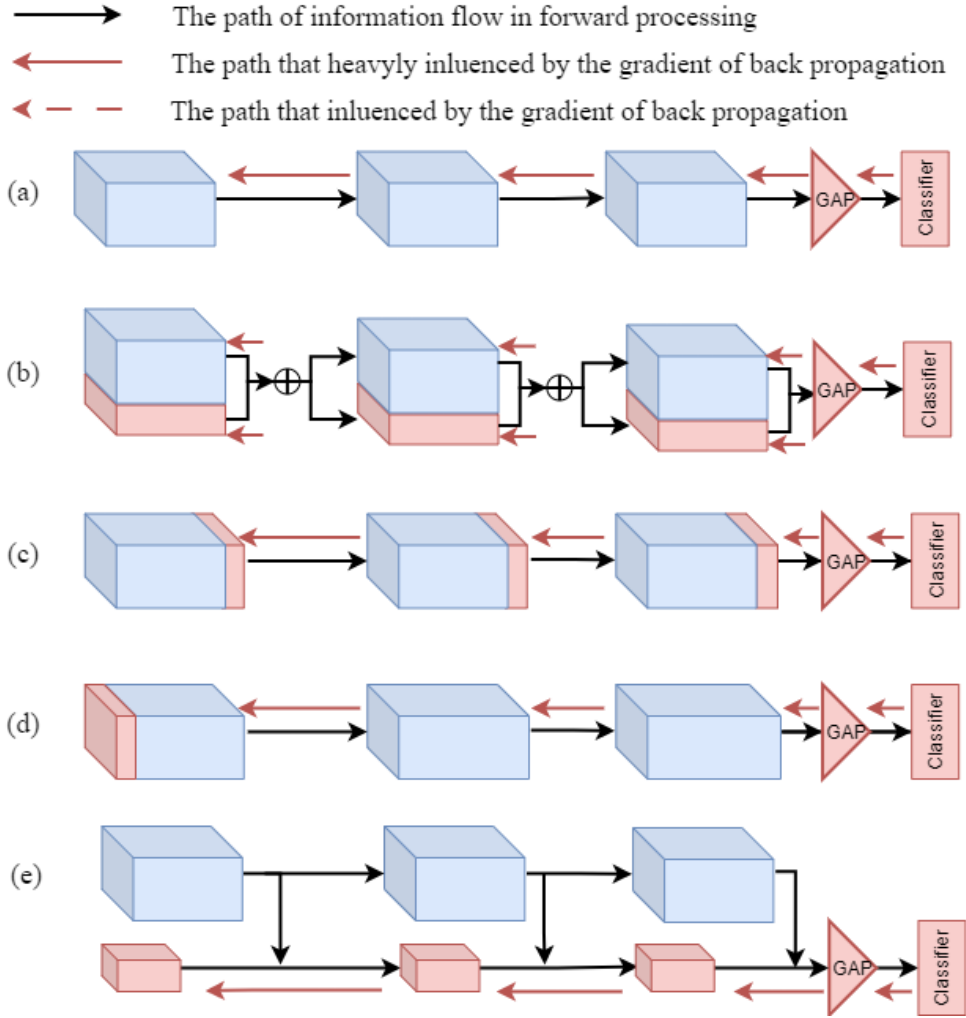


Figure 1: Comparison of different fine tuning architectures. (a) FPFT; (b) Adapter tuning; (c) LoRA; (d) Prompt tuning; (e) Ladder side tuning.

3.1. Primary introduction of ViT model

ViT is a representative vanilla visual transformer model. It directly processes images as sequences of patches, and then utilizes self-attention mechanisms to capture long-range dependencies between these patches. The self-attention operation computes a weighted sum of the embeddings based on their pairwise relationships, which can be expressed as follows:

$$Attention(Q, K, V) = \text{softmax} \left(\frac{QK^T}{\sqrt{d_k}} + P \right) V \quad (1)$$

where Q, K, V are the query, key, and value matrices, respectively, representing the input embeddings. d_k denotes the dimensionality of V , and P means relative position embedding (RPB),

$$P_{(x,y),(x',y')}^h = Q_{(x,y),:} \cdot K_{(x',y'),:} + B_{|x-x'|,|y-y'|}^h \quad (2)$$

where B^h represents the translation-invariant attention bias.

Based on self-attention operation, the multi-head attention layer can be constructed. Each transformer block consists of two sub-layers: a Multi-Head Self-Attention (MHSA) layer (token mixer) and a Feed-Forward Neural Network (FFN)

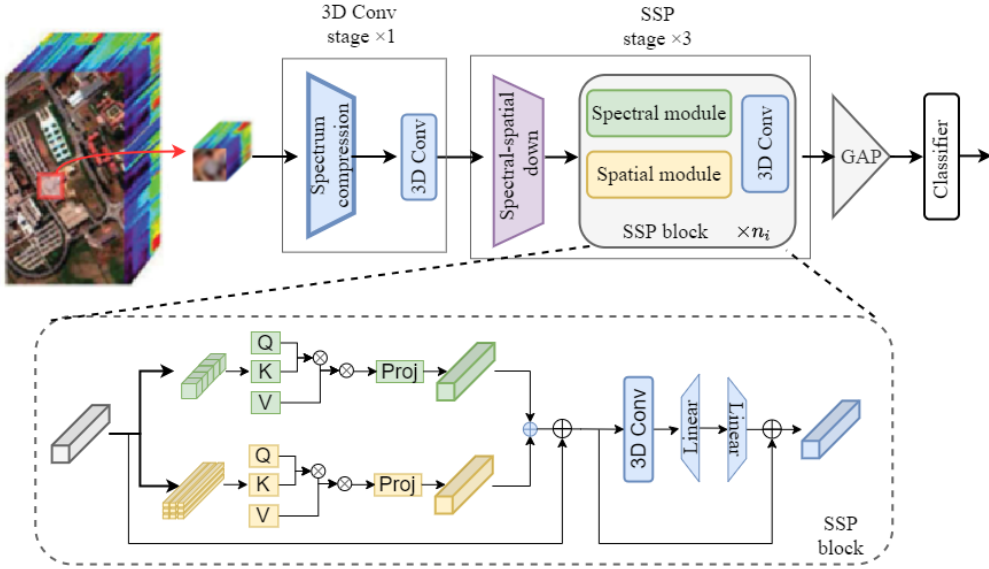


Figure 2: Architecture of proposed Tri-Former. SSP block has three main parts, spectral module, spatial module and 3D convolution module, which is why we call it triplet-structured. Spectral module is responsible for collecting information from different spectrum bands. Spatial module is in charge of collecting information from different space locations. 3D convolution layer is added before the two linear layers to enforce 3D structure information and stabilize training process.

layer (channel mixer). The output of each transformer block is then fed to the subsequent block, enabling hierarchical feature extraction.

Apart from the aforementioned layer, the ViT model also includes a special learnable positional embedding that encodes the position information of each patch in the image sequence. Two common methods of adding position embedding are: 1) applying RPB to the attention map, as in Eq.1; 2) adding absolute position embedding to the patch embeddings. In the vanilla ViT model, preserving positional information is crucial. However, employing position embeddings can be a bit cumbersome, especially when there are changes in the input patch resolution.

3.2. Architecture of Tri-Former

To efficiently learn features from limited annotated samples, Tri-Former emphasizes improving architectural flexibility and reducing redundant computations. By analyzing the spatial-spectral characteristics of HSIs, we propose Tri-Former, a triplet-structured transformer designed specifically for HSI classification. Tri-Former employs the spectral-spatial parallel architecture to tackle computational inefficiencies and incorporates 3D convolution to enhance structural information.

Overall architecture. As is depicted in Figure 2. The overall framework consists of four stages, including one 3D convolution stage and three transformer stages, as shown in the top half of Figure 2. Stage one comprises a spectrum compression module and a 3D convolution module. The subsequent three stages are constructed with the proposed spectral-spatial parallel (SSP) blocks. Each stage begins with a spectral-spatial downsample layer, followed by n_i SSP blocks. Following the classical design strategy, the widths of the four stages are progressively doubled from stage to stage. In this work, the width of the first stage is set to 32 as the starting point for subsequent widening. This design choice enables the network to efficiently process and extract relevant information in a computationally efficient manner.

Spectral-spatial parallel block. SSP block first compresses the spectral dimension of input feature. After that, each feature map $f \in \mathbb{R}^{e \times s \times w \times h}$ is splitted to sequence and input to the spatial module and spectral module. Specifically, in the spectral module, the spectral query, spectral key, and spectral value can be expressed as:

$$Q_e \in \mathbb{R}^{R_e \times N_e \times L_e}, \quad K_e \in \mathbb{R}^{R_e \times N_e \times L_e}, \quad V_e \in \mathbb{R}^{R_e \times N_e \times L_e}, \quad (3)$$

where $R_e = h \times w$, $N_e = s$, $L_e = c$. The corresponding spectral attention feature is:

$$Atten_{spe} = \text{LN} \left(\frac{\text{softmax}(Q_e \cdot K_e^T)}{\sqrt{d_e}} \cdot V_e \right), \quad (4)$$

where softmax is conducted along the last dimension, \cdot denotes matrix multiplication and it is conducted along the last two dimension. In the spatial module, the spatial attention feature $Atten_{spa}$ is calculated following the same equation, but the input feature is splitted in different ways. Specifically, the spatial query, spatial key, and spatial value can be represented as:

$$Q_a \in \mathbb{R}^{R_a \times N_a \times L_a}, \quad K_a \in \mathbb{R}^{R_a \times N_a \times L_a}, \quad V_a \in \mathbb{R}^{R_a \times N_a \times L_a}, \quad (5)$$

where $R_a = s$, $N_a = h \times w$, $L_a = c$. The computing process in SSP block can be formalized as Eq.6 and Eq.7:

$$f_{ssp} = f + \text{reshape}(Atten_{spe}, \mathbb{R}^{c \times s \times w \times h}) + \text{reshape}(Atten_{spa}, \mathbb{R}^{c \times s \times w \times h}), \quad (6)$$

$$f_{out} = \text{MLP}(\text{Conv}(f_{ssp})) + f_{ssp} \quad (7)$$

where $\text{reshape}(\cdot, \mathbb{R}^{c \times s \times w \times h})$ means reshape the input feature to $\mathbb{R}^{c \times s \times w \times h}$. LN and MLP means linear layer and multilayer perceptron.

In Eq.7, a 3D convolution is employed. Such a design has two advantages: 1) this additional 3D convolution contributes to stabilize the optimization process of the transformer block; 2) it enhances the structure information (position information) and obviates the necessity to rely on position embedding in the original ViT.

After the sequential 3D Conv and SSP stages, the learned features are transformed into feature vectors using global average pooling (GAP). Finally, a classifier is used to generate the final prediction.

Analysis on computational complexity. The proposed spectral-spatial parallel (SSP) block significantly reduces the computation cost. Instead of directly applying self-attention on three dimensions (two spatial dimensions and one spectral dimension), spectral and spatial information are separately processed. The computation complexity of the vanilla ViT is quantic complex regarding to the length of the input sequence. In 3D architecture HSI, this issue is more serious. As shown in Figure 3, for a input feature $f \in \mathbb{R}^{c \times s \times w \times h}$, if we directly compute self-attention on three dimensions, the computation complexity is:

$$O(\text{VANILLA}(f)) = O(h^2 w^2 s^2 c) \quad (8)$$

where VANILLA denotes the vanilla transformer architecture that directly applies self-attention on three dimensions. In the proposed SSP architecture, the computational complexity becomes:

$$O(\text{SSP}(f)) = O(h^2 w^2 s c) + O(h w s^2 c) \quad (9)$$

In practical experiments, the value of c and s are relatively large, making $O(\text{SSP}(f))$ significantly smaller than $O(\text{VANILLA}(f))$. For instance, if the input feature map has a spatial size of 27×27 , with 32 channels and 144 spectral bands. $O(\text{SSP}(f)) = O(2.93 \times 10^9)$, while $O(\text{VANILLA}(f)) = O(3.53 \times 10^{11})$.

Obviously, the designed SSP block significantly reduces computational load, rendering the entire architecture more lightweight and adaptable, This beneficial to feature learning on HSIs with limited annotations.

Analysis on receptive field. The enhancements on transformer architecture have significant impacts on their receptive field. The receptive field in the proposed SSP block excludes certain irrelevant elements within its scope, consequently strengthening the attention on pixels with close relationships. Using two-dimensional features as an example, we illustrate the receptive fields of SSP block and that of vanilla transformer in Figure 3. From Figure 3(b), it is evident that the receptive field of the vanilla structure is a square region. But as in Figure 3(a), the proposed SSP block considers pixels that share the same row, column, or spatially adjacent positions with the central pixel. The self-attention operation in the ViT architecture achieves information fusion by computing approximate similarities between each pair of pixels. However, when a pixel is relatively distant from the central pixel, it may not effectively contribute to extracting information from the central pixel. Thus, retaining such distant pixels within the receptive field may indeed introduce noise. Therefore, the receptive field of our proposed module retains only the most crucially related pixels, while excluding irrelevant interference pixels, resulting in a more efficient mechanism.

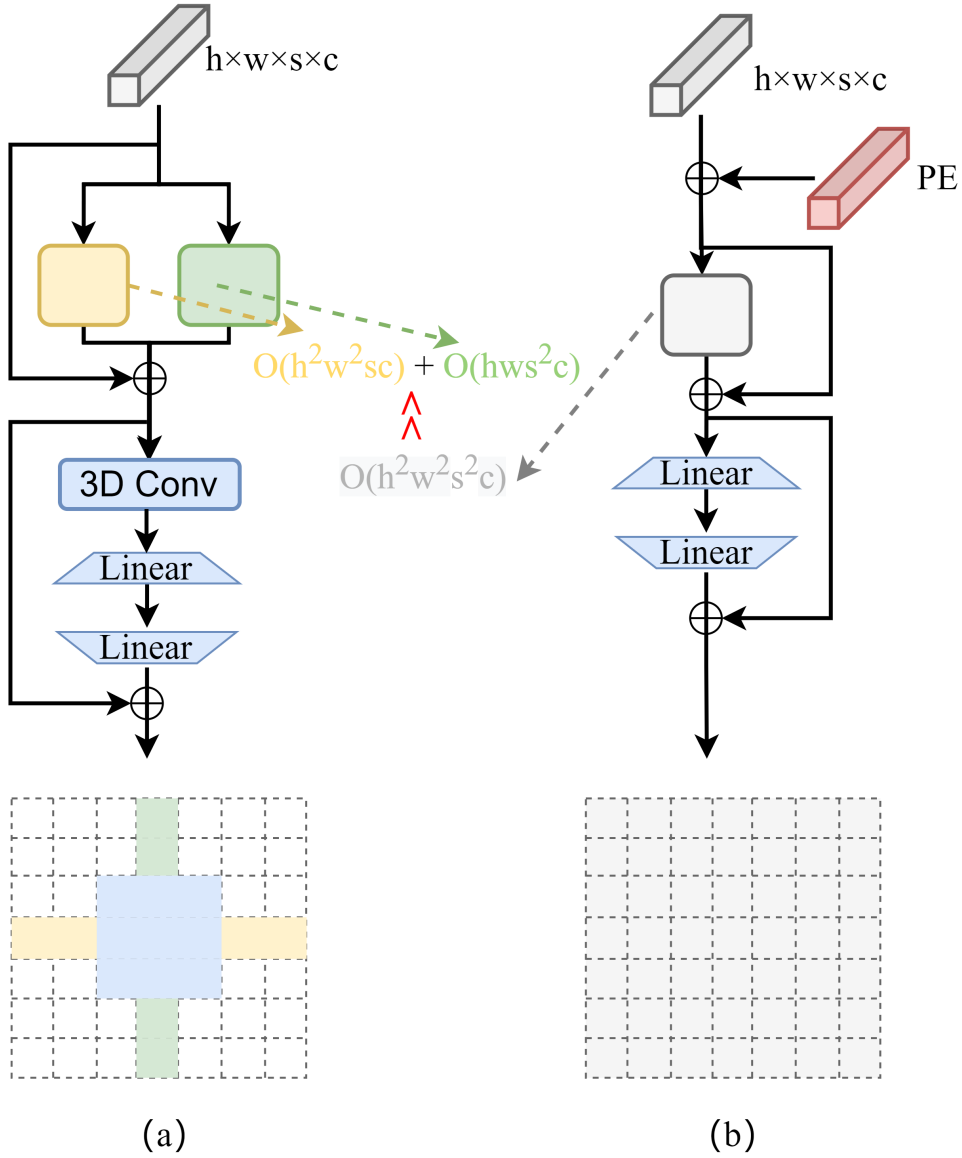


Figure 3: Comparison between proposed SSP block and vanilla ViT block. (a) SSP block; (b) Vanilla ViT block.

3.3. Attention-Gated Tuning

Attention-Gated Tuning (AGT) is proposed to enable a transformer-based HSI classification method to leverage cross-sensor or cross-modality data to further enhance performance. As illustrated in Figure 4, AGT serves as a bridge, bridging the gaps between target HSIs and images captured by other sensors. The process of AGT is consists of two sequential stages:

- Firstly, the basic model is pretrained with homogeneous and heterogeneous hyperspectral data, even RGB data, as illustrated in the blue part of Figure 4. It is worth noting that there is a significant modal disparity between RGB data and hyperspectral data. Therefore, we initially generate pseudo-hyperspectral data from RGB data to mitigate these modality gaps. Specifically, we employ DRCR-Net¹ to create the 32-channel pseudo-HSI data from RGB data Li et al. (2022) and then use these pseudo-HSIs to perform pretraining, as depicted in Figure 5. These generated images possess certain spectral characteristics while harnessing the advantages of extensive

¹<https://github.com/jojolee6513/DRCR-net>

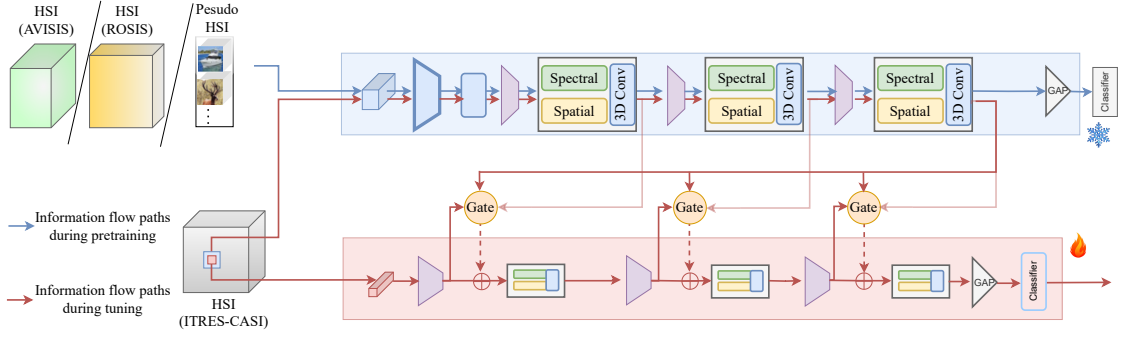


Figure 4: Architecture of proposed AGT. Blue part is the basic model, where big patches and heavy Tri-Former are adopted. Red part is an auxiliary branch, where a small patch and tiny Tri-Former are used.

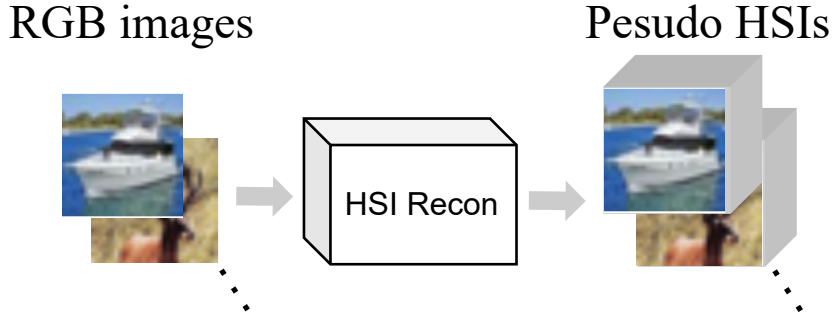


Figure 5: Framework of generating pseudo HSIs data from RGB images.

natural image data. Experimental results in Section 4.8 demonstrate that the AGT can also benefit from RGB data.

- Secondly, a tiny auxiliary branch is introduced to the basic model before tuning on the target HSI datasets, as presented in the Figure 4. Corresponding to the n_i blocks in the basic model, the auxiliary branch consists of n_i lightweight SSP blocks. To reduce the overhead associated with the auxiliary branch, we choose smaller patches, shallower architectures, and narrower modules. Through an attention-gated strategy, the proposed AGT can autonomously select useful information from the basic model to guide auxiliary branch learning. Unlike previous fine tuning methods Jia et al. (2022); Liu et al. (2023, 2021); Sung et al. (2022), where the basic model remains frozen during tuning, we employ an asynchronous cold-hot gradient update strategy, in which the basic model is updated slowly.

In terms of design, AGT has three notable aspects that guarantee its effective functioning in our scenario. To elaborate further:

- **Parallel architecture.** In the proposed AGT approach, a tiny auxiliary branch is introduced and updated to adapt to the target datasets. This modification arises from the acknowledgment that distinct HSI datasets exhibit more pronounced variations when compared to the disparities between diverse RGB datasets. Incorporating only a limited number of new learnable parameters within the basic model has proven insufficient for effectively bridging this gap. Such a parallel architecture offers two distinct advantages. Firstly, during the tuning process, detaching the foundational model from gradient updating becomes effortless, enabling a more controlled adjustment. This adjustment aligns perfectly with the requirements for fine tuning the transformer model for HSI classification. Secondly, the architectural design of the auxiliary branch is more flexible.
- **Attention-guided learning.** In the proposed AGT, features from each stage of the basic model are introduced to guide the auxiliary branch learning. Specifically, as shown in Figure 6, f_{bas} and f_{end} denote the feature

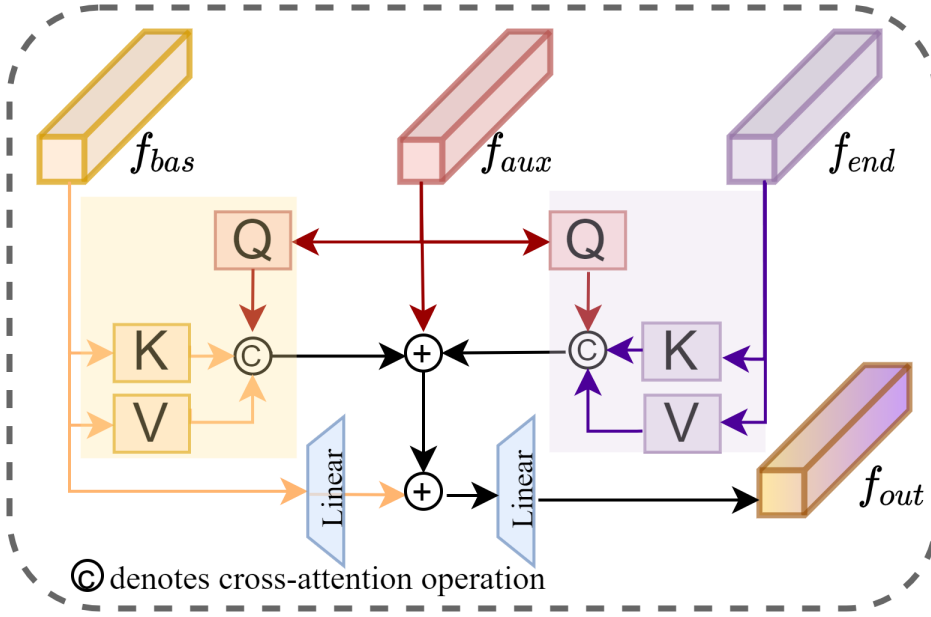


Figure 6: Workflow of proposed attention gate.

from current stage and last stage of basic model, respectively. Shallow features contain an excess of detailed information, whereas deep features encompass more semantic information. AGT combines shallow and deep features learned from pre-training to provide stronger guidance for HSI classification tasks. The gating mechanism is achieved through cross-attention, as shown in Figure 6. This approach allow the auxiliary branch to selectively fuse useful information from the basic model while filtering out conflict information learned during pretraining.

- **Asynchronous cold-hot gradient update strategy.** From comprehensive experiments, we find that completely freezing the foundational model as what is done in RGB image processing and NLP fields Jia et al. (2022); Liu et al. (2023) does not work well in HSI classification. We speculate that this phenomenon arises due to the significant disparities among different HSI datasets. Therefore, a more suitable approach involves gradually fine tuning the basic model, allowing it to adjust appropriately and accommodate new data. Therefore, we propose an asynchronous cold-hot gradient update strategy, where **basic model** is updated slowly (**cold**) and the **auxiliary branch** is updated quickly (**hot**).

Although the design of AGT is inspired by the core idea of ladder side tuning (LST) Jia et al. (2022), their motivations, key problems, architectures and gradient updating are totally different. 1) AGT aims to alleviate limited label sample problems in HSI classification, whereas LTS focuses on fine tuning large language models (LLM); 2) AGT deals with HSIs collected by various sensors or even datasets from different domains. LST is proposed for datasets from the same modality; 3) AGT uses information from the auxiliary branch to guide feature fusion, which reuse the features from the current stage and the end stage; 4) As depicted in Figure 7(b), AGT employ a cold-hot gradient update strategy , while LST always freeze the basic model. The corresponding experiments in Section IV.E demonstrate the effectiveness of proposed AGT.

4. Experiments

4.1. Data Description

In order to make a comprehensive comparison, Indian Pines dataset, Pavia University dataset and Houston University dataset are used in the experiments. The sample distribution information is listed in Table 1.

Indian Pines dataset was acquired by the Airborne Visible/Infrared Imaging Spectrometer (AVIRIS) sensor during a flight campaign over the Indian Pines agricultural site in Indiana, USA. The Indian Pines dataset consists of a HSI with a high spectral resolution, capturing information in 224 contiguous spectral bands covering the wavelength range

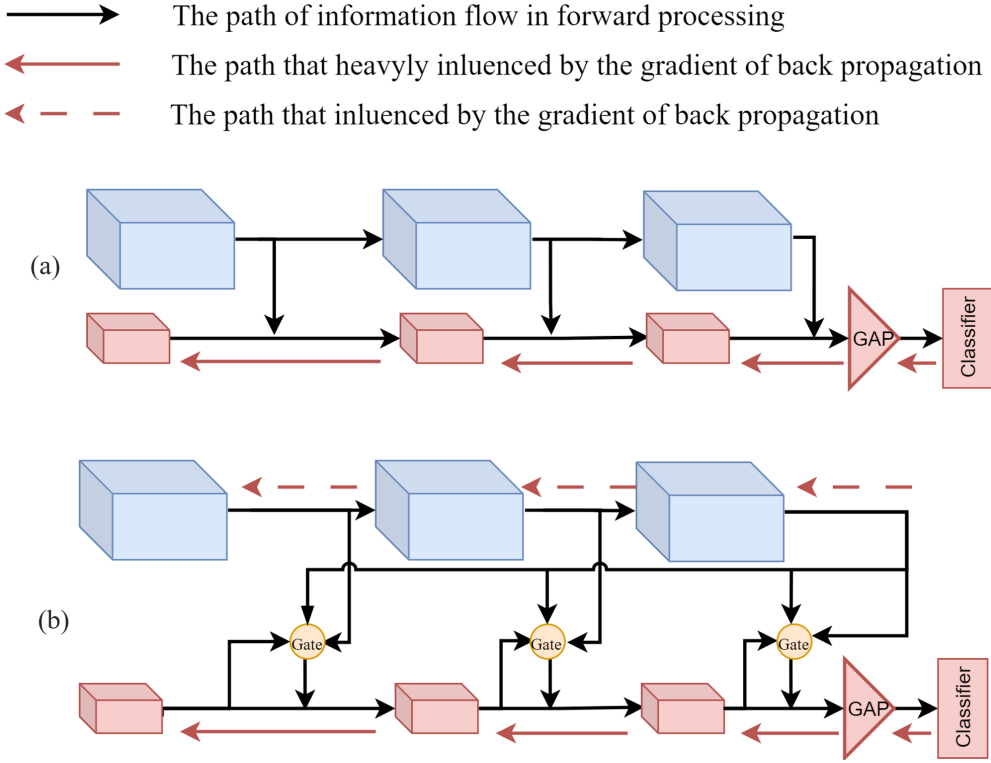


Figure 7: Architecture comparison on proposed AGT and related work. (a). LST; (b). AGT.

from 0.4 μm to 2.5 μm . The spatial resolution of the dataset is 145 \times 145 pixels, making it relatively small compared to some other hyperspectral datasets. The primary objective of the Indian Pines dataset is to classify the various land-cover objects present in the agricultural area, which includes crops, bare soil, and different types of vegetation. The dataset contains 16 different land-cover classes in total.

Pavia University dataset was collected by the Reflective Optics System Imaging Spectrometer (ROSIS) sensor during a flight campaign over Pavia, a city in northern Italy. The dataset consists of a HSI with a high spectral resolution and geometric resolution of 1.3 meters. It captures information in 103 contiguous spectral bands covering the wavelength range from 0.43 μm to 0.86 μm . The spatial resolution of the Pavia University dataset is 610 \times 340 pixels, making it of moderate size. The dataset contains 9 land-cover classes, representing various ground objects and materials present in the urban and agricultural regions of Pavia. The main objective of the Pavia University dataset is to classify the different land-cover classes present in the scene, which includes urban areas, vegetation, soil, and other materials.

Houston University dataset was captured by the ITRES-CASI 1500 hyperspectral imager over the University of Houston campus and the neighboring urban area in June 2012. The dataset comprises a HSI with a high spectral resolution, covering 144 contiguous spectral bands that span the wavelength range from 0.36 μm to 1.05 μm . With a spatial resolution of 349 \times 1905 pixels, the Houston University dataset is relatively large, providing a detailed representation of the urban and suburban regions in the vicinity of the university. Houston University dataset consists of 349 \times 1905 pixels. The dataset encompasses 15 distinct land-cover classes, including urban structures, roads, vegetation, water bodies, and other land-use categories typically encountered in urban environments.

4.2. Experiment Design

The experimental setup encompasses two comparative segments for classification evaluation. The first part involves basic model comparison experiments, while the second focuses on comparing various tuning strategies.

In the basic model comparison part, we partition each target HSI dataset into two subsets: the training set and test set. We randomly extract 150 samples from each category as test samples and take the rest as the training samples in the Pavia University dataset and Houston University. For the Indian Pines dataset, we sample a small number of pixels from

Table 1
Sample distribution information of Datasets

Indian Pines			Pavia University		Houston University	
Class	Land Cover Type	No.of Samples	Land Cover Type	No.of Samples	Land Cover Type	No.of Samples
1	Alfalfa	46	Asphalt	6631	Healthy Grass	1251
2	Corn-notill	1428	Meadows	18649	Stressed Grass	1254
3	Corn-mintill	830	Gravel	2099	Synthetic Grass	697
4	Corn	237	Trees	3064	Trees	1244
5	Grass-pasture	483	Painted Metal Sheets	1345	Soil	1242
6	Grass-trees	730	Bare Soil	5029	Water	325
7	Grass-pasture-mowed	28	Bitumen	1330	Residential	1268
8	Hay-windrowed	478	Self-Blocking Bricks	3682	Commercial	1244
9	Oats	20	Shadows	947	Road	1252
10	Soybean-notill	972	-	-	Highway	1227
11	Soybean-mintill	2455	-	-	Railway	1235
12	Soybean-clean	593	-	-	Parking Lot 1	1233
13	Wheat	205	-	-	Parking Lot 2	469
14	Woods	1265	-	-	Tennis Court	428
15	Buildings-Grass-Trees-Drives	386	-	-	Running Track	660
16	Stone-Steel-Towers	93	-	-	-	-
Total		10249	Total	42776	Total	15029

classes with scarce samples to ensure a more balanced representation for the experiments. Concretely, we randomly select 10 samples from each of the following six classes: Alfalfa (class 1), Grass/trees (class 5), Grass/pasture-mowed (class 7), Oats (class 9), Buildings-grass-trees (class 15), and Stone-steel towers (class 16). For the remaining classes, we sample 150 pixels from each class. In this Section 4.4, we compare our proposed Tri-Former model with other state-of-the-art algorithms.

In addition, we compare the proposed AGT approach with other popular tuning methods on HSIs collected from different sensors. The tuning strategies comparison results are presented in Section 4.6 and Section 4.7. These experiments involve data from two source sensors: Salinas (captured by AVIRIS) and Pavia Center (captured by ROSIS). For the model trained on the data collected by one sensor, we fine-tune it on the target data collected by another sensor with a limited number of samples. We design different experimental groups, each containing 25, 50, and 75 labeled pixels per class, respectively. Furthermore, in Section 4.8, we evaluate the proposed method by cross-modality fine tuning experiments. Specifically, the basic Tri-Former model pretrained on RGB images is finetuned on different HSI datasets with different tuning method.

Through comprehensive and systematic experiments, we demonstrate the effectiveness of the proposed method in addressing HSI classification. To ensure the fairness and stability of the comparison, we repeat each experiment five times and take the average values as the final results.

4.3. Implementation Details and Evaluation Metrics

Implementation details: The optimization of the proposed method consists of two stages. The entire learning process is conducted on the server with 4 NVIDIA 3090 GPUs. During training, the training samples are cropped as 27x27 spatial resolution patches, with a batch size of 96 on all three training dataset. We utilize the AdamW optimizer with a learning rate and weight decay value of 1×10^{-3} and 1×10^{-5} , respectively. The learning rate decays from 1×10^{-3} to 1×10^{-6} following the cosine scheduler. The warming-up stage comprises 5 epochs and all the models are trained for 300 epochs. To further tune the final network, we crop patches with spatial resolutions of 13x13 and 27x27, which are fed into the auxiliary branch and basic model, respectively. Batch sizes are set to 12 for all datasets during tuning.

4.4. Comparison between Tri-Former and state-of-the-art methods

In this section, we conduct a comparative analysis of our proposed Tri-Former against five ConvNet-based and transformer-based HSI classification methods. The comparisons are based on official implementations of these methods: 3D-CNN² Chen et al. (2016), LWNet³ Zhang et al. (2019), SpectralFormer⁴ Hong et al. (2021), GraphGST⁵ Jiang

²<https://github.com/eeen/Hyperspectral-Classification>

³<https://github.com/hkzhang91/LWNet>

⁴https://github.com/danfenghong/IEEE_TGRS_SpectralFormer

⁵<https://github.com/yuanchaosu/TGRS-graphGST>

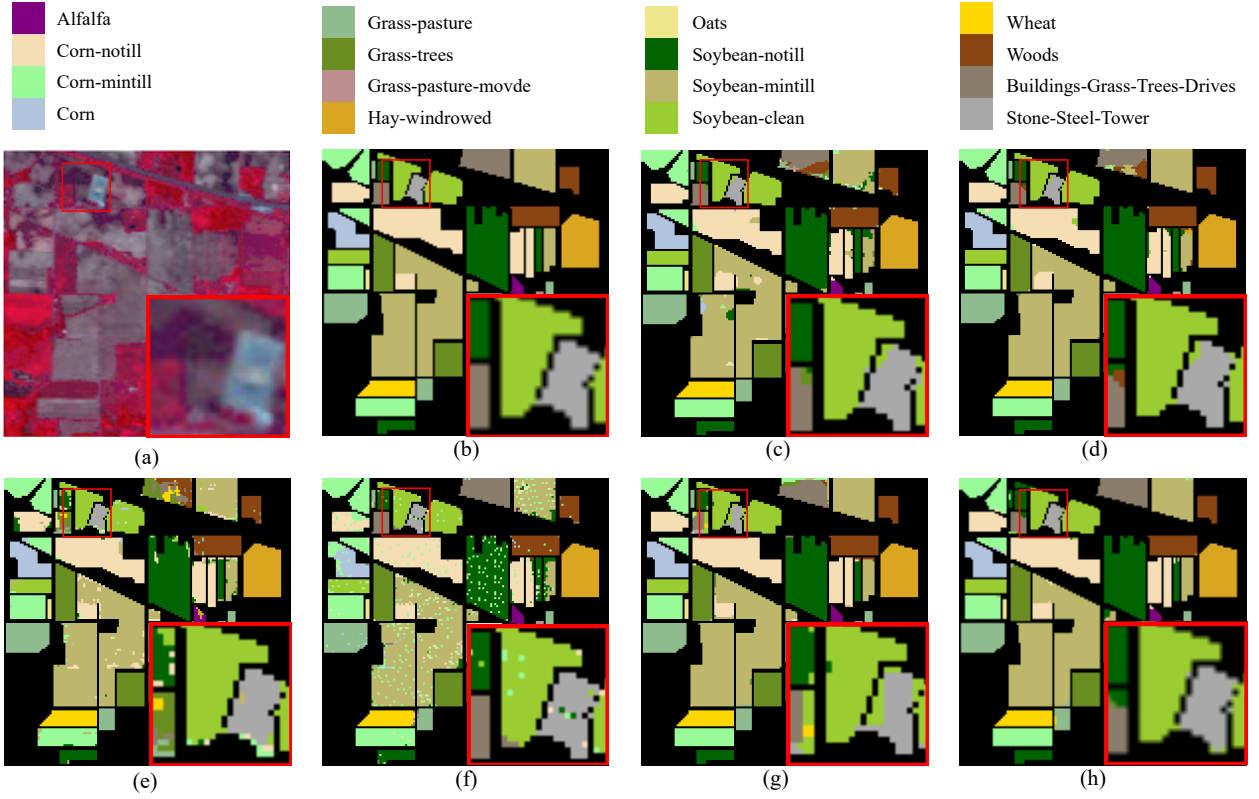


Figure 8: Results on Indian Pines dataset. (a) Composite color map; (b) Ground truth; (c) 3D-CNN; (d) LWNet; (e) SpectralFormer; (f) GraphGST; (g) SSFTT; (h) Tri-Former.

et al. (2024) and SSFTT⁶ Sun et al. (2022). The experimental results are presented in Table 2 to Table 4, and the visual comparisons are shown in Figure 8 to Figure 10.

The quantitative analysis results of the aforementioned approaches on the Indian Pines dataset are listed in Table 2. Table 2 shows that the proposed Tri-Former achieves the highest OA of 98.41%, outperforming other ConvNet-based HSI classification methods like 3D-CNN (95.23%), LWNet (97.46%), SpectralFormer (93.08%), GraphGST (96.02%) and SSFTT (97.12%). Among them, SSFTT incorporation of convolutional operations within the transformer structure, which benefits its performance. This improvement further substantiates some of the points we have mentioned in this work. Introducing convolutional operations to construct hybrid transformer models for processing HSI is a more suitable approach. The proposed Tri-Former further improved the OA metric of SSFTT by 1.29%, demonstrating its remarkable capability to accurately classify HSIs in this challenging dataset.

Figure 8 shows the corresponding visual results. At the top, a color-composite image is presented, accompanied by color codes that represent different types of ground objects. The bottom-right corner features a magnified view, aimed at providing a clearer comparison of the classification performance of different methods. From Figure 8, we can see that all methods exhibit varying degrees of misclassification. Our proposed Tri-Former demonstrates the least amount of misclassification, approaching the ground truth closely.

Similar trends are also demonstrated in the experiments conducted on the Pavia University and Houston University datasets. When evaluated on the Pavia University dataset, the proposed Tri-Former algorithm surpasses the state-of-the-art method SSFTT, achieving remarkable improvements in key evaluation metrics. Specifically, we observe substantial enhancements in Overall Accuracy (OA), Average Accuracy (AA), and Kappa (K) coefficient by 1.85%, 1.71%, and 2.45%, respectively. On the Houston University dataset, where the potential for performance improvement is considerably limited, our Tri-Former still manages to achieve the best performance among all methods compared.

⁶https://github.com/zgr6010/HSI_SSFTT

Table 2

Comparison Experimental Results on Indian Pines Using 150 Training Samples Each Class

Models	3D-CNN	LWNet	SpectralFormer	GraphGST	SSFTT	Tri-Former
1	91.67	97.22	77.78	100.00	100.00	97.14
2	94.84	96.01	90.06	94.91	94.99	99.45
3	99.12	98.82	94.26	99.26	99.12	99.71
4	100.00	100.00	98.85	74.89	100.00	100.00
5	100.00	100.00	99.10	96.99	100.00	91.45
6	100.00	99.83	98.97	97.76	99.83	100.00
7	100.00	100.00	94.44	94.44	100.00	100.00
8	100.00	100.00	100.00	100.00	100.00	100.00
9	100.00	100.00	100.00	100.00	100.00	100.00
10	99.39	100.00	96.35	99.15	99.51	99.51
11	92.41	98.39	90.54	93.02	95.05	98.13
12	98.42	99.77	96.61	96.61	99.55	99.56
13	100.00	100.00	100.00	97.95	100.00	100.00
14	98.92	99.91	98.92	99.46	98.82	100.00
15	66.49	70.74	68.35	100.00	89.63	91.76
16	90.36	91.57	84.33	97.59	83.13	89.16
OA	95.23	97.46	93.08	96.02	97.12	98.41
AA	95.73	97.02	93.04	96.38	97.54	97.87
K	94.47	97.05	91.97	95.41	96.66	98.17

Table 3

Comparison Experimental Results on Pavia University Using 150 Training Samples Each Class

Models	3D-CNN	LWNet	SpectralFormer	GraphGST	SSFTT	Tri-Former
1	91.09	96.06	83.13	98.06	94.69	99.98
2	92.05	95.69	92.83	98.03	98.74	99.91
3	92.45	95.95	89.34	92.82	98.50	100.00
4	98.55	98.68	97.60	99.11	95.05	99.18
5	99.52	99.92	100.00	100.00	97.43	100.00
6	93.14	98.09	90.32	90.92	99.96	100.00
7	97.48	99.76	96.99	100.00	100.00	99.92
8	95.20	99.11	92.63	95.95	99.08	99.77
9	97.28	98.82	99.65	99.74	99.88	100.00
OA	93.26	96.86	91.65	98.06	98.03	99.88
AA	95.20	98.01	93.61	98.18	98.15	99.86
K	91.13	95.84	89.00	97.41	97.38	99.83

Figure 9 and Figure 10 are the corresponding visual comparison results. On these two datasets, especially on the Pavia University dataset, the proposed Tri-Former produces classification result maps that closely resemble the groundtruth.

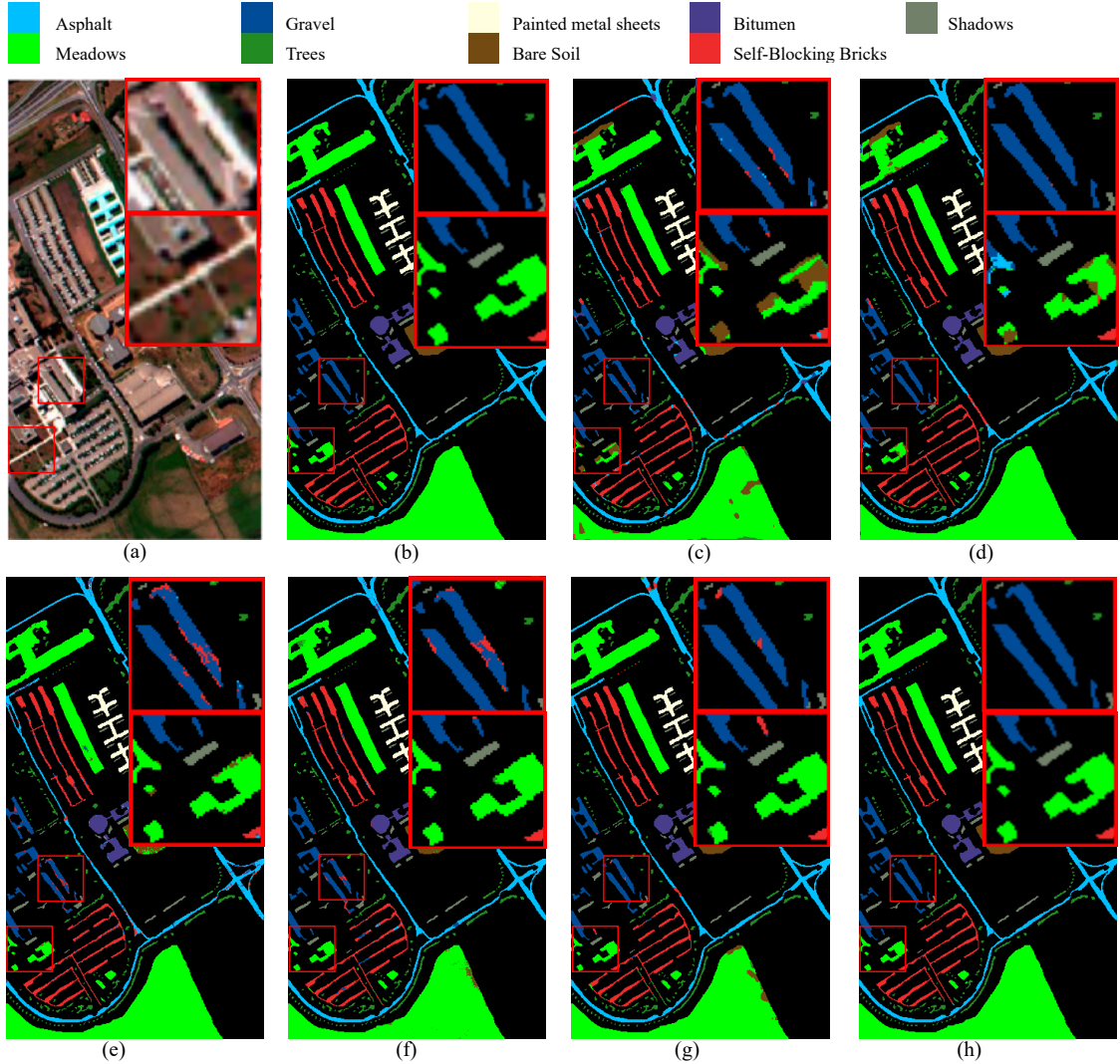


Figure 9: Results on Paiva University. (a) Composite color map; (b) Ground truth; (c) 3D-CNN; (d) LWNet; (e) SpectralFormer; (f) GraphGST; (g) SSFTT; (h) Tri-Former.

4.5. Inference speed analysis on Tri-Former

To comprehensively evaluate the complexity and the inference speed of the proposed Tri-Former model, we conducted a thorough comparison between Tri-Former and two other recent, representative transformer-based HSI classification methods: SpectralFormer and SSFTT.

In this section, we ran each model 10 times on the same dataset and averaged the number of pixels processed per second. The experimental results are shown in Figure 11, which demonstrate that the proposed Tri-Former enjoy clear advantages in both classification accuracy and inference speed. Compared with SSFTT, Tri-Former achieves 3× faster inference speed, while maintaining advantage in classification accuracy. On the Houston University dataset, Tri-Former improves classification accuracy by 10% compared to SpectralFormer while also achieving about a 20% increase in inference speed.

4.6. Comparison between AGT and state-of-the-art methods

For evaluating the effectiveness of the proposed AGT strategy, we conducted a comprehensive comparison with several representative architecture tuning methods. The comparison methods involved in the evaluation are as follows: Fine-tune (adopted in LWNet Zhang et al. (2019) and Two-CNN Yang et al. (2017) for ConvNet methods), LORA Hu et al. (2022), Clip-adapter Gao et al. (2021) and LST Sung et al. (2022) (for transformer methods).

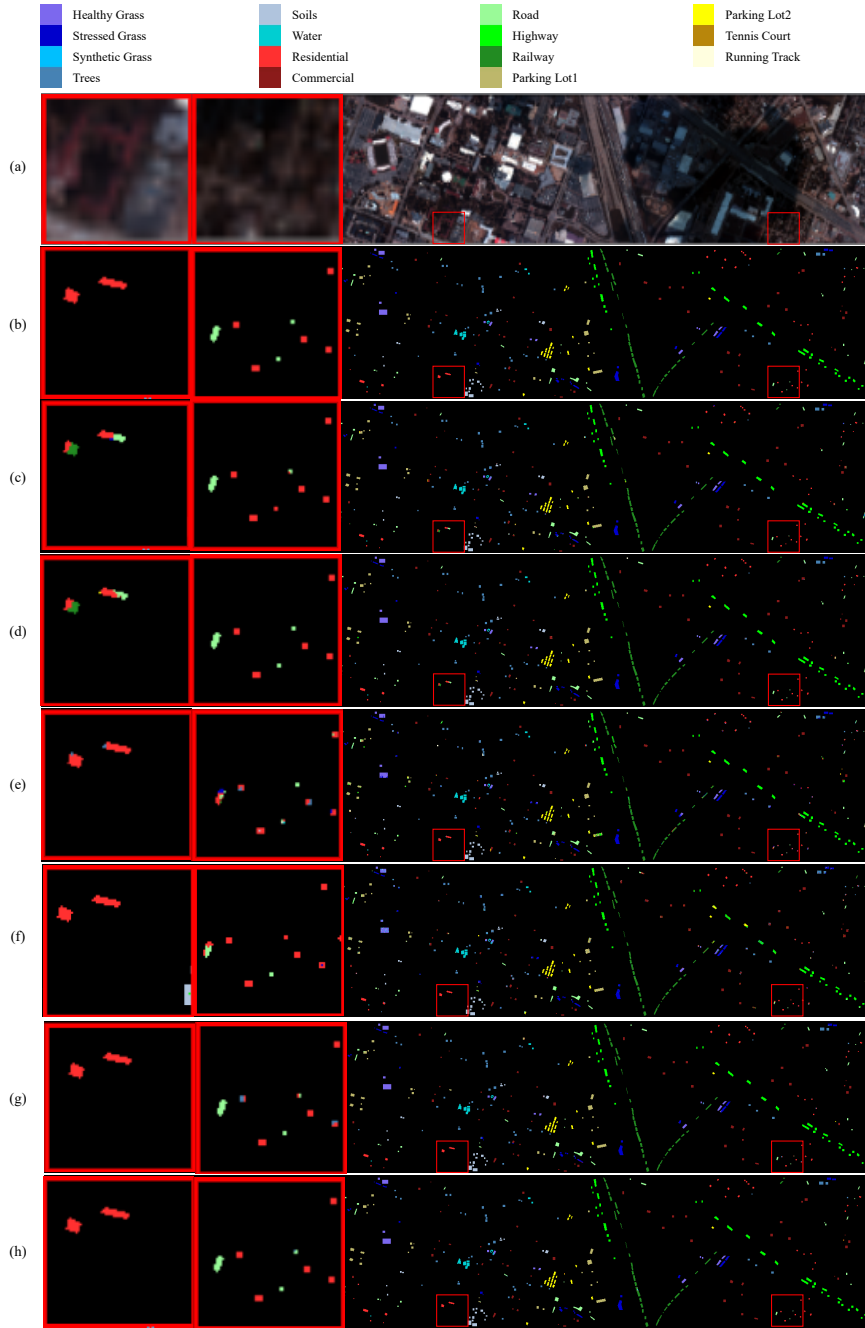


Figure 10: Results on Houston University. (a) Composite color map; (b) Ground truth; (c) 3D-CNN; (d) LWNNet; (e) SpectralFormer; (f) GraphGST; (g) SSFTT; (h) Tri-Former.

In this experiment, the basic model is first pretrained on the Salinas dataset acquired through the AVRIS sensor. In this process, 50 labeled pixels are randomly extracted from each class to build a pretraining set. Then, the model is fine-tuned with various strategies on three distinct target datasets captured by different sensors: AVRIS, ROSIS and ITRES-CASI. Within the tuning stage, each class is provided with 50 training samples. The experimental results are consolidated in Figure 12, where the x-axis denotes the employed tuning methods and the y-axis depicts the evaluation metric. According to the comparison, we can draw four conclusions:

Table 4

Comparison Experimental Results on Houston University Using 150 Training Samples Each Class

Models	3D-CNN	LWNet	SpectralFormer	GraphGST	SSFTT	Tri-Former
1	96.64	98.64	96.00	78.47	98.00	99.64
2	95.20	99.01	89.31	83.51	97.10	97.92
3	99.82	100.00	99.09	84.82	99.09	100.00
4	97.62	99.54	86.47	79.43	97.90	99.73
5	99.45	100.00	95.88	97.43	100.00	99.91
6	100.00	100.00	86.86	88.57	100.00	100.00
7	91.68	96.06	73.23	62.88	98.66	99.11
8	94.70	96.71	85.56	54.39	97.62	97.17
9	96.82	97.19	85.57	54.38	99.82	98.82
10	98.33	99.44	91.55	70.10	100.00	99.63
11	97.05	100.00	92.35	51.34	100.00	97.05
12	96.12	98.25	86.98	60.85	96.21	100.00
13	95.61	100.00	82.45	86.20	99.37	100.00
14	100.00	100.00	100.00	94.96	100.00	100.00
15	100.00	100.00	97.65	86.67	100.00	100.00
OA	96.58	98.70	89.19	94.42	98.69	99.05
AA	97.14	98.99	89.93	95.13	98.92	99.26
K	96.29	98.59	88.28	93.94	98.57	98.97

- **Conventional fine tuning strategy tailored for ConvNets proves ineffective on the cross-sensor HSI data.**

As shown in Figure 12, the Fine-tune strategy not only fails to yield any improvement but also negatively affects the final results. We hypothesize that this phenomenon can be attributed to the fundamental differences between the information learned by ConvNets and transformer architectures. ConvNets learn a set of filter parameters from the training data. The process of feature extraction in ConvNets is static. Differing from this, transformer architectures learn relationships between pixels, capturing global dependencies in the data. The transformer is a data-driven model with a dynamic feature extraction process, making it more sensitive to differences between the pretraining dataset and the new target dataset. Unfortunately, there are obvious differences among cross-sensor HSI datasets, which consequently hinder the effectiveness of fine tuning.

- **Tuning strategies proposed for transformer architecture have a certain role on cross-sensor HSI data.**

LORA and Clip-adaptor are specifically designed for transformer-based algorithms, and they do achieve higher classification accuracy compared to fine tuning methods tailored for CNNs. However, despite their overall performance advantage, these two fine tuning methods still exhibit negative effects in certain experiments. We speculate the reason is that the pretrained basic model is heavily influenced during the tuning stage. When the adaptor introduces significant changes to the basic model during fine tuning, the fine-tuned model may lose some of the informative features learned during pre-training. As a result, the performance of LORA and Clip-adaptor could be negatively impacted in certain scenarios, particularly when there are a lot of differences between the pre-training and fine tuning datasets. Significant updating of the basic model's parameters may disrupt the underlying spectral-spatial patterns captured during pre-training, leading to a drop in classification accuracy.

- **Freezing the basic model is not always effective.** As shown in Figure 12, LST does not perform well in *Salines*→*Houston University* experiment, whereas it brings in certain improvements in the other two experiments. We speculate that this issue arises from the LST strategy, which does not update the gradients of the basic model. While this approach preserves the features learned during pre-training, it is not always beneficial when there are significant differences in data structure, such as the number of bands. In such cases, the pre-trained

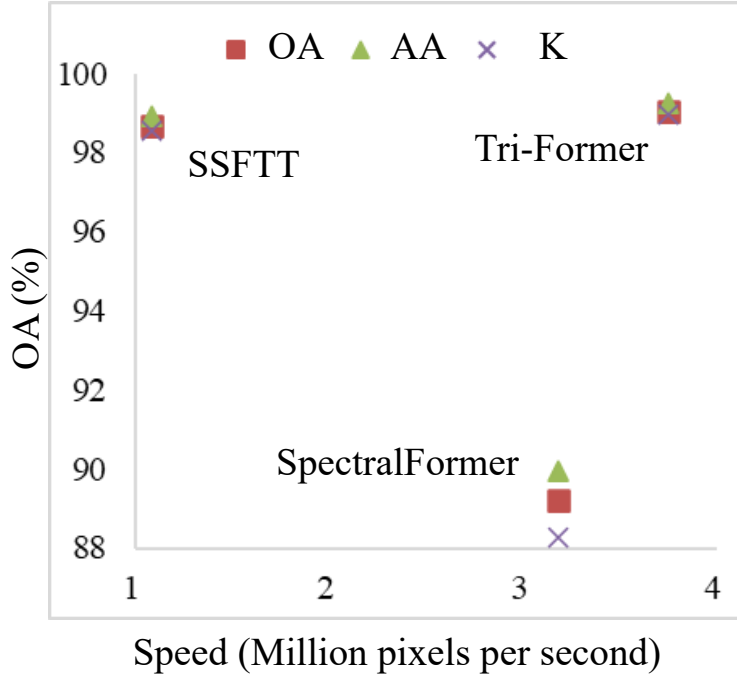


Figure 11: Comparison results on classification accuracy and inference speed.

knowledge may conflict with the target dataset. These conflicting representations are not adjusted during LST fine tuning, leading to performance drop.

- **Proposed AGT works well.** Experimental results have shown that information selection and gradient updates during fine tuning are crucial. Benefiting from the attention-gated block and cold-hot gradient update strategy, AGT ensures that the fine tuning process adapts the model to the target dataset, while preserving the generic spectral-spatial representations learned during pre-training. This approach contributes to its superior performance in various experimental scenarios, even when faced with cross-sensor data.

4.7. Experiments on homogeneous and heterogeneous HSI datasets

To further validate the effectiveness of the proposed method and investigate the influence of homogeneity and heterogeneity on tuning experiments, we conducted two sets of experiments on the Indian Pines, Salinas, Pavia University, and Pavia Center datasets. The first two datasets, Indian Pines and Salinas, are homogeneous and captured by AVIRIS, while the last two, Pavia University and Pavia Center, are homogeneous and captured by ROSIS. In the first set of experiments, the basic model was pretrained on the Salinas dataset and fine-tuned on the Indian Pines and Pavia University datasets under three configurations: 25, 50, and 75 training samples per class. The experimental results depicted in the radar charts in Figure 13 show that:

- **AGT boosts performance across all the experimental settings.** Whether in a homogeneous or heterogeneous scenario, employing AGT consistently leads to a significant improvement in accuracy, which once again proves the effectiveness of our attention-gated strategy.
- **Transferring between homogeneous datasets offers more advantages than transferring between heterogeneous datasets.** Even Pavia Center dataset contains only ten classes and has less sample diversity compared to Salinas dataset with 16 classes, the advantages of *Pavia Center*→*Pavia University* tuning are more obvious than *Salinas*→*Pavia University* tuning. This phenomenon shows that when fine tuning transformer models, the similarity between pretrain and target datasets is likely to be important than the diversity of the pretrain dataset itself. This differs from previous experiences with fine tuning ConvNets. Researchers Zhang et al. (2019) found that for ConvNets, the diversity of the pretrain data is more important than its homogeneity. We speculate this

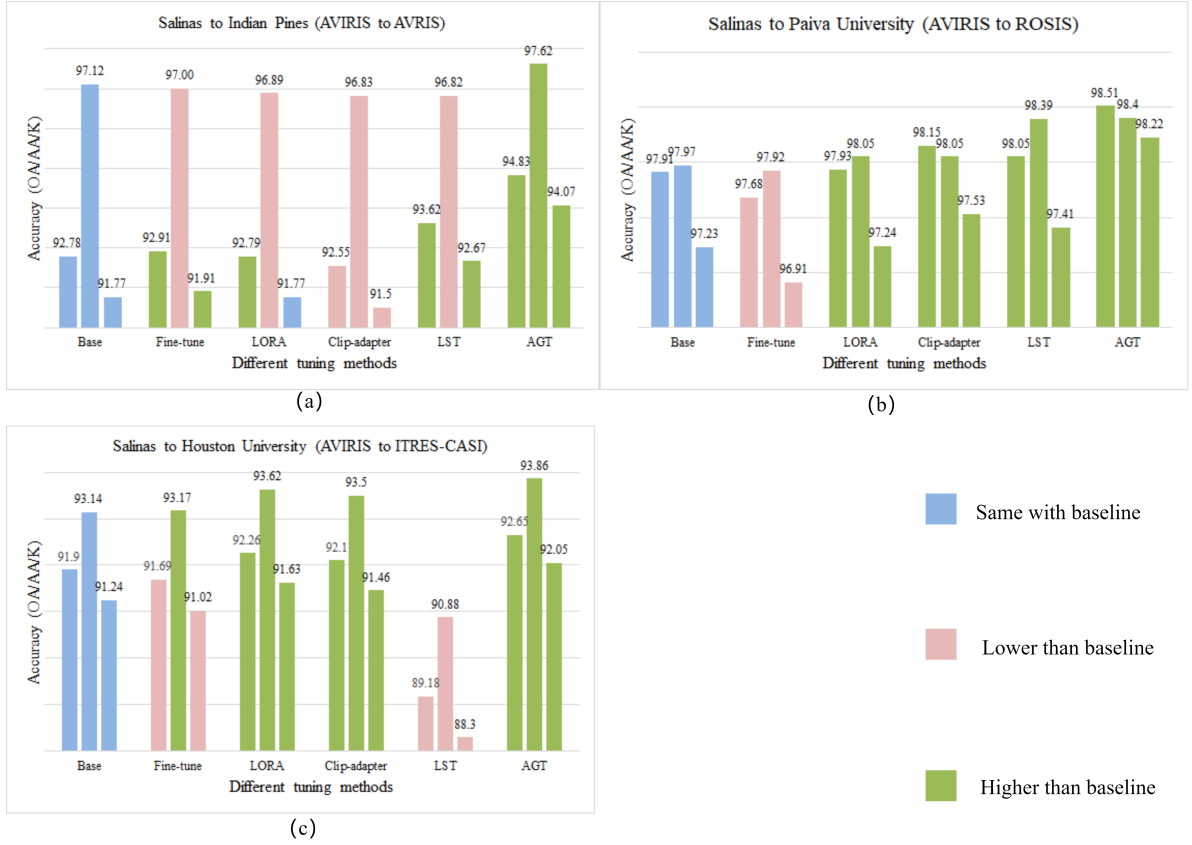


Figure 12: Comparison of different tuning methods.

is because transformers learn dependencies between pixels in the dataset, while ConvNets learn static filter parameters from the data. Therefore, fine tuning transformers requires higher homogeneity between pretrain and fine tuning data.

4.8. Using AGT as a bridge between RGB datasets and HSI datasets

RGB data is abundant and highly diverse. The barrier between RGB and HSI datasets is that they are cross-modality datasets. In this section, we combine HSI reconstruction method and the proposed AGT to build a bridge to cross this barrier.

More specifically, a pretrained HSI reconstruction model Li et al. (2022) is applied to convert 3-channel RGB image to 32-channel pseudo-HSIs. Then the pseudo-HSIs are used to pretrain the basic model. The RGB dataset used here is CIFAR⁷. We randomly extract 25 samples from each category as tuning samples and take the rest as the testing samples. Experimental results are listed in Table 5.

Interestingly, in this setting, AGT achieves results that are as good as, or even superior to, those obtained with homogenous data. Cross-modality experiments can be viewed as a further extension of cross-sensor experiments. At first glance, this experimental result seems contradictory to the previous results. We suspect that the main reason for this phenomenon is the strong sample diversity of the CIFAR dataset, which offsets the effects of heterogeneous data to some extent. This is essential for remote sensing applications with expensive data collection costs.

Just as mentioned in our method, the proposed AGT serves as a bridge to address the modal differences between RGB datasets and HSI datasets. This is crucial, particularly considering the presence of datasets with even greater sample diversity in the realm of RGB datasets. The bridge allows us to make use of these datasets. Additionally, to enhance the HSI classification performance, larger models are required. Larger labeled datasets are necessary for

⁷<https://www.cs.toronto.edu/~kriz/cifar.html>

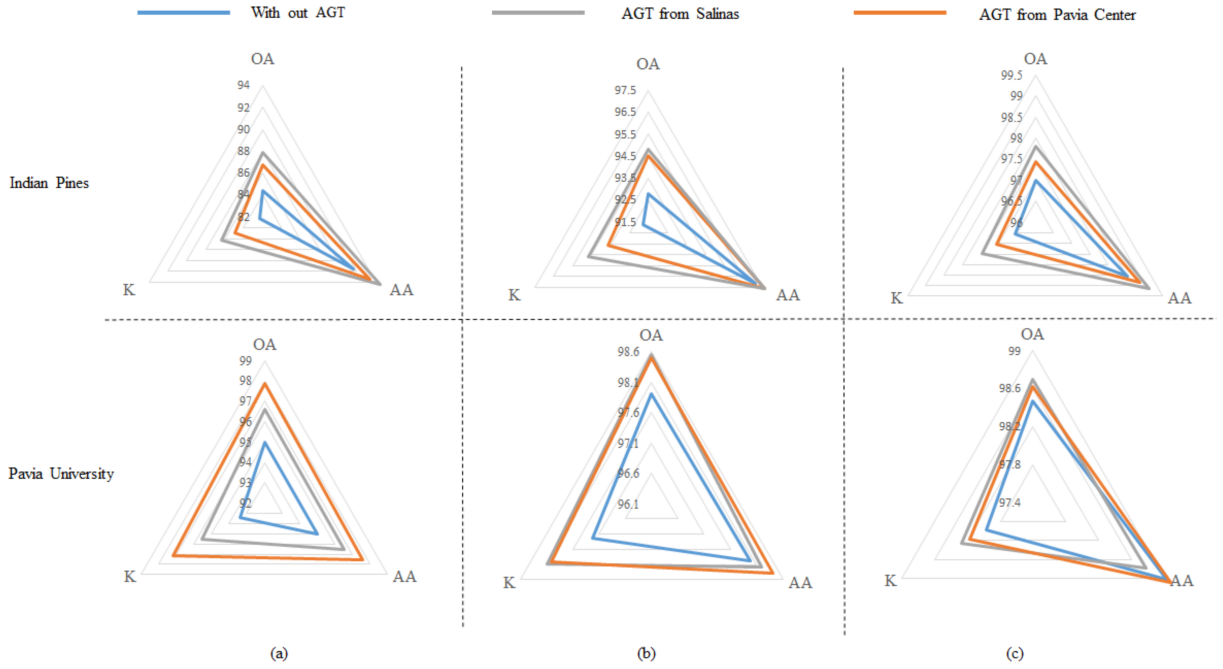


Figure 13: Experimental results on homogeneous and heterogeneous HSI datasets. (a) 25 training samples per class; (b) 50 training samples per class; (c) 75 training samples per class.

Table 5
Experimental Results of Cross Sensors Transfer Learning from RGB Data

Dataset	Indian pines			PaviaU			HoustonU		
Sensor	RGB→ AVIRIS			RGB→ ROSIS			RGB → ITRES-CASI		
Method	Base	LST	AGT	Base	LST	AGT	Base	LST	AGT
OA	84.36	70.14	86.14	95.00	81.05	95.08	83.00	71.00	85.14
AA	91.64	83.33	93.85	95.03	81.21	95.40	84.34	75.06	87.17
K	82.28	66.46	84.35	93.40	75.43	93.61	81.64	68.72	83.96

training these larger models. AGT provides a way to effectively leverage existing RGB datasets to enhance the accuracy of HSI classification.

4.9. Visual analysis on attention gate

In this section, we investigate whether the proposed attention gate can select relevant features from the basic model to enhance the features in the auxiliary branch. Specifically, following the inference process, we feed a large patch into the basic model and crop a smaller patch from its center to input into the auxiliary branch. The corresponding visual results are presented in Figure 14.

The visual results demonstrate that the attention gate functions passing relevant features selectively. If we directly connected the basic model and auxiliary branch, all features in the basic model be equally selected. Alternatively, if the proposed attention mechanism could not guide information flow from the basic model to the auxiliary branch, the selection map would appear random. However, Figure 14 shows that features from the basic model highly relevant to those in the auxiliary branch are selectively chosen. This observation underscores the effectiveness of the attention gate mechanism in fine tuning HSI classification methods.

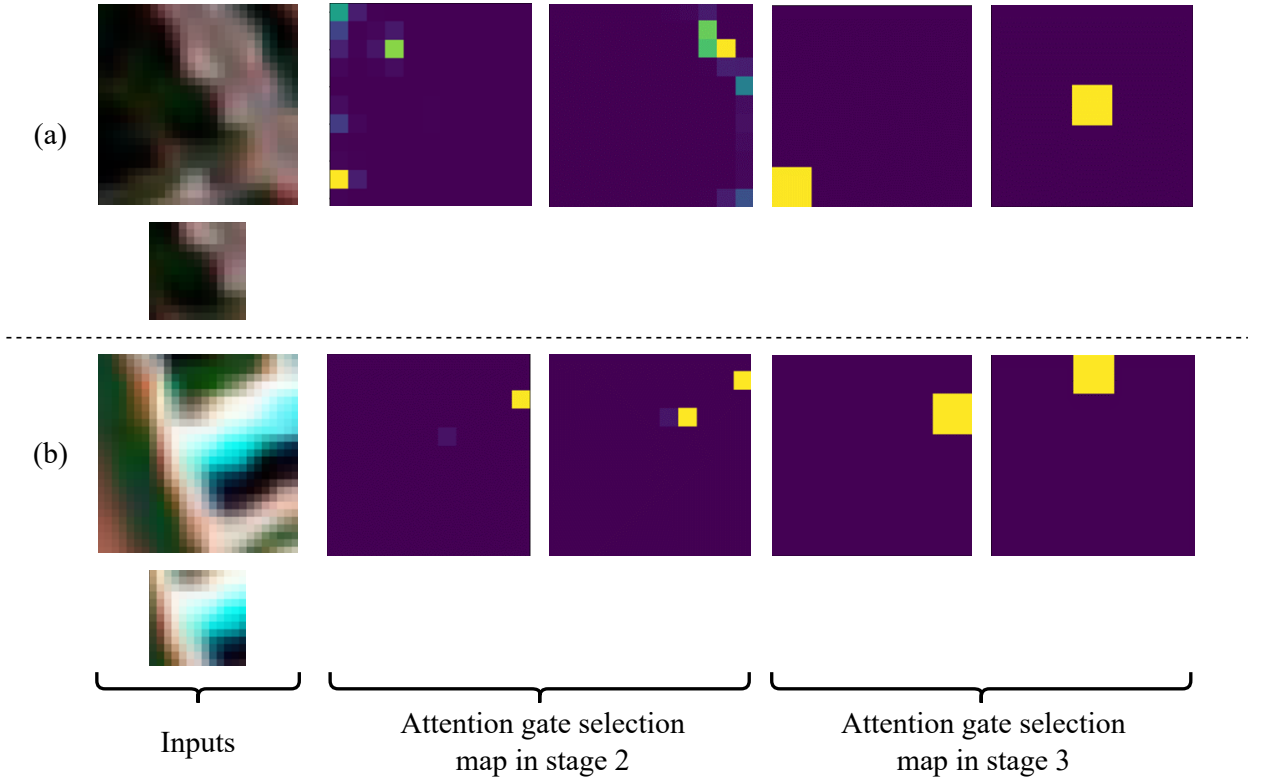


Figure 14: Visual results of the gate attention selection process. (a) and (b) are two different samples.

5. Conclusion

In this paper, to effectively diminish the demand for an extensive quantity of training samples, we propose the attention gated tuning (AGT) strategy. Acting as a bridge, AGT enables us to capitalize on both pre-existing labeled HSI datasets and even RGB datasets, thereby enhancing the performance on new HSI datasets with constrained sample sizes. Furthermore, we have presented the triplet-structured transformer (Tri-Former) model for HSI classification. By introducing spectral-spatial parallel block, Tri-Former optimizes computational efficiency while enhancing model stability. Extensive experiments across diverse HSI datasets and sensors verified the proposed Tri-Former. Homologous, heterologous, and cross-modality tuning experiments are conducted to validate the performance of the proposed AGT. We hope this research can inspire the designs of fine tuning methods in HSI classification and guide the selection of pre-training datasets.

References

- Behmann, J., Steinrücken, J., Plümer, L., 2014. Detection of early plant stress responses in hyperspectral images. *ISPRS Journal of Photogrammetry and Remote Sensing* 93, 98–111.
- Carrino, T.A., Crósta, A.P., Toledo, C.L.B., Silva, A.M., 2018. Hyperspectral remote sensing applied to mineral exploration in southern peru: A multiple data integration approach in the chapi chiara gold prospect. *International journal of applied earth observation and geoinformation* 64, 287–300.
- Chen, Y., Jiang, H., Li, C., Jia, X., Ghamisi, P., 2016. Deep feature extraction and classification of hyperspectral images based on convolutional neural networks. *IEEE Trans. Geosci. Remote Sens.* 54, 6232–6251.
- Chen, Y., Lin, Z., Zhao, X., Wang, G., Gu, Y., 2014. Deep learning-based classification of hyperspectral data. *IEEE J. Sel. Topics Appl. Earth Observ. Remote Sens.* 7, 2094–2107.
- Chen, Y., Zhao, X., Jia, X., 2015. Spectral-spatial classification of hyperspectral data based on deep belief network. *IEEE J. Sel. Topics Appl. Earth Observ. Remote Sens.* 8, 2381–2392.
- Chen, Y., Zhu, K., Zhu, L., He, X., Ghamisi, P., Benediktsson, J.A., 2019. Automatic design of convolutional neural network for hyperspectral image classification. *IEEE Transactions on Geoscience and Remote Sensing* 57, 7048–7066.

- Dosovitskiy, A., Beyer, L., Kolesnikov, A., Weissenborn, D., Zhai, X., Unterthiner, T., Dehghani, M., Minderer, M., Heigold, G., Gelly, S., et al., 2020. An image is worth 16x16 words: Transformers for image recognition at scale. arXiv preprint arXiv:2010.11929 .
- Gao, P., Geng, S., Zhang, R., Ma, T., Fang, R., Zhang, Y., Li, H., Qiao, Y., 2021. Clip-adapter: Better vision-language models with feature adapters. arXiv preprint arXiv:2110.04544 .
- He, K., Zhang, X., Ren, S., Sun, J., 2016. Deep residual learning for image recognition, in: Proc. IEEE Conf. Comput. Vis. Pattern Recognit. (CVPR), pp. 770–778.
- He, X., Chen, Y., Lin, Z., 2021. Spatial-spectral transformer for hyperspectral image classification. Remote Sensing 13, 498.
- Hong, D., Han, Z., Yao, J., Gao, L., Zhang, B., Plaza, A., Chanussot, J., 2021. Spectralformer: Rethinking hyperspectral image classification with transformers. IEEE Transactions on Geoscience and Remote Sensing .
- Howard, A.G., Zhu, M., Chen, B., Kalenichenko, D., Wang, W., Weyand, T., Andreetto, M., Adam, H., 2017. Mobilenets: Efficient convolutional neural networks for mobile vision applications. arXiv preprint arXiv:1704.04861 .
- Hu, E.J., Shen, Y., Wallis, P., Allen-Zhu, Z., Li, Y., Wang, S., Wang, L., Chen, W., 2022. LoRA: Low-rank adaptation of large language models, in: International Conference on Learning Representations. URL: <https://openreview.net/forum?id=nZeVKeeFYf9>.
- Huang, G., Liu, Z., Weinberger, K.Q., van der Maaten, L., 2017. Densely connected convolutional networks, in: Proc. IEEE Conf. Comput. Vis. Pattern Recognit. (CVPR), p. 3.
- Jia, M., Tang, L., Chen, B.C., Cardie, C., Belongie, S., Hariharan, B., Lim, S.N., 2022. Visual prompt tuning, in: European Conference on Computer Vision, Springer. pp. 709–727.
- Jiang, M., Su, Y., Gao, L., Plaza, A., Zhao, X.L., Sun, X., Liu, G., 2024. Graphgst: Graph generative structure-aware transformer for hyperspectral image classification. IEEE Transactions on Geoscience and Remote Sensing 62, 1–16. doi:10.1109/TGRS.2023.3349076.
- Krizhevsky, A., Sutskever, I., Hinton, G.E., 2012. Imagenet classification with deep convolutional neural networks, in: Proc. Adv. Neural Inf. Process. Syst., pp. 1097–1105.
- Lester, B., Al-Rfou, R., Constant, N., 2021. The power of scale for parameter-efficient prompt tuning, in: Proceedings of the 2021 Conference on Empirical Methods in Natural Language Processing, pp. 3045–3059.
- Li, J., Du, S., Wu, C., Leng, Y., Song, R., Li, Y., 2022. Drccr net: Dense residual channel re-calibration network with non-local purification for spectral super resolution, in: Proceedings of the IEEE/CVF conference on computer vision and pattern recognition, pp. 1259–1268.
- Li, Y., Zhang, H., Shen, Q., 2017. Spectral–spatial classification of hyperspectral imagery with 3d convolutional neural network. Remote Sensing 9, 67.
- Lin, Z., Chen, Y., Zhao, X., Wang, G., 2013. Spectral-spatial classification of hyperspectral image using autoencoders, in: 2013 9th International Conference on Information, Communications & Signal Processing, IEEE. pp. 1–5.
- Liu, P., Yuan, W., Fu, J., Jiang, Z., Hayashi, H., Neubig, G., 2023. Pre-train, prompt, and predict: A systematic survey of prompting methods in natural language processing. ACM Computing Surveys 55, 1–35.
- Liu, X., Ji, K., Fu, Y., Tam, W.L., Du, Z., Yang, Z., Tang, J., 2021. P-tuning v2: Prompt tuning can be comparable to fine-tuning universally across scales and tasks. arXiv preprint arXiv:2110.07602 .
- Liu, Z., Mao, H., Wu, C.Y., Feichtenhofer, C., Darrell, T., Xie, S., 2022. A convnet for the 2020s. Proceedings of the IEEE/CVF Conference on Computer Vision and Pattern Recognition (CVPR) .
- Makantasis, K., Karantzalos, K., Doulamis, A., Doulamis, N., 2015. Deep supervised learning for hyperspectral data classification through convolutional neural networks, in: Proc. IEEE Conf. Int. Geosci. Remote Sens. Symp (IGARSS), pp. 4959–4962.
- Mei, S., Ji, J., Bi, Q., Hou, J., Du, Q., Li, W., 2016. Integrating spectral and spatial information into deep convolutional neural networks for hyperspectral classification, in: Proc. IEEE Conf. Int. Geosci. Remote Sens. Symp (IGARSS), pp. 5067–5070.
- Pan, S.J., Yang, Q., 2009. A survey on transfer learning. IEEE Transactions on knowledge and data engineering 22, 1345–1359.
- Qing, Y., Liu, W., Feng, L., Gao, W., 2021. Improved transformer net for hyperspectral image classification. Remote Sensing 13, 2216.
- Simonyan, K., Zisserman, A., 2014. Very deep convolutional networks for large-scale image recognition. arXiv preprint arXiv:1409.1556 .
- Sun, L., Zhao, G., Zheng, Y., Wu, Z., 2022. Spectral–spatial feature tokenization transformer for hyperspectral image classification. IEEE Transactions on Geoscience and Remote Sensing 60, 1–14.
- Sung, Y.L., Cho, J., Bansal, M., 2022. Lst: Ladder side-tuning for parameter and memory efficient transfer learning. Advances in Neural Information Processing Systems 35, 12991–13005.
- Szegedy, C., Ioffe, S., Vanhoucke, V., Alemi, A.A., 2017. Inception-v4, inception-resnet and the impact of residual connections on learning., in: Proc. AAAI Conf. Intell., p. 12.
- Transon, J., d’Andrimont, R., Maignard, A., Defourny, P., 2018. Survey of hyperspectral earth observation applications from space in the sentinel-2 context. Remote Sensing 10, 157.
- Vaswani, A., Shazeer, N., Parmar, N., Uszkoreit, J., Jones, L., Gomez, A.N., Kaiser, Ł., Polosukhin, I., 2017. Attention is all you need, in: Advances in neural information processing systems, pp. 5998–6008.
- Xue, X., Zhang, H., Fang, B., Bai, Z., Li, Y., 2022. Grafting transformer on automatically designed convolutional neural network for hyperspectral image classification. IEEE Transactions on Geoscience and Remote Sensing 60, 1–16. doi:10.1109/TGRS.2022.3180685.
- Yang, J., Zhao, Y.Q., Chan, J.C.W., 2017. Learning and transferring deep joint spectral–spatial features for hyperspectral classification. IEEE Trans. Geosci. Remote Sens. 55, 4729–4742.
- Yue, J., Zhao, W., Mao, S., Liu, H., 2015. Spectral–spatial classification of hyperspectral images using deep convolutional neural networks. Remote Sensing Letters 6, 468–477.
- Zhang, H., Gong, C., Bai, Y., Bai, Z., Li, Y., 2021. 3-d-anas: 3-d asymmetric neural architecture search for fast hyperspectral image classification. IEEE Transactions on Geoscience and Remote Sensing 60, 1–19.
- Zhang, H., Li, Y., 2016. Spectral-spatial classification of hyperspectral imagery based on deep convolutional network, in: 2016 International Conference on Orange Technologies (ICOT), IEEE. pp. 44–47.

- Zhang, H., Li, Y., Jiang, Y., Wang, P., Shen, C., 2019. Hyperspectral classification based on lightweight 3-d-cnn with transfer learning. *IEEE Transactions on Geoscience and Remote Sensing* 57, 5813–5828.
- Zhang, H., Li, Y., Zhang, Y., Shen, Q., 2017. Spectral-spatial classification of hyperspectral imagery using a dual-channel convolutional neural network. *Remote sensing letters* 8, 438–447.
- Zhang, J.O., Sax, A., Zamir, A., Guibas, L., Malik, J., 2020. Side-tuning: a baseline for network adaptation via additive side networks, in: *Computer Vision—ECCV 2020: 16th European Conference, Glasgow, UK, August 23–28, 2020, Proceedings, Part III* 16, Springer. pp. 698–714.
- Zhong, Z., Li, J., Luo, Z., Chapman, M., 2018. Spectral-spatial residual network for hyperspectral image classification: A 3-d deep learning framework. *IEEE Trans. Geosci. Remote Sens.* 56, 847–858.